

After this the polymer was rigid and could be peeled off carefully from the silicon master.

The suspensions were prepared by adding powder to distilled water under constant stirring. The pH was always kept between 4 and 5 by dropwise adding a 2 M solution of hydrochloric acid (Titrisol, Merck, Darmstadt, Germany). Thereafter the suspensions were ball milled with alumina milling balls for 18 h. Two drops of 1-octanol (puriss, Fluka, Buchs, Switzerland) were added to reduce the surface tension of the suspension before degassing for 15 min at 90 mbar under constant rotation.

For the formation of the ceramic samples a few drops of the particle suspension were poured onto the PDMS template and dried in room atmosphere. No separating agent was applied onto the mold. The suspension layer on the template structure was kept relatively thin (about 1 mm) in respect to its diameter (about 5 mm) to get quasi uniaxial shrinkage in the thickness direction to prevent high lateral shrinking rates during drying. After drying, the ceramic parts were carefully lifted from the molds and sintered. The PDMS templates were cleaned in an ultrasonic bath after processing and could be reused. The alumina samples were heated with 300 K/h to 1550 °C and held there for 3 h. The boehmite samples were heated with 300 K/h to 300 °C, then with 60 K/h to 600 °C to allow the phase transition of boehmite from γ -AlOOH to γ -Al₂O₃ and then with 300 K/h to 1250 °C and held there for 4 h.

Suspensions of three powders with different particle sizes were prepared. Their properties are listed in Table 2. For a good pattern replication the suspensions needed to have a relatively low viscosity of about 0.5 Pa s which limits the amount of powder that can be dispersed. The achieved solids loadings decreased with decreasing particle size of the powders. Solids loadings in volume percent are shown in Table 2.

Table 2. Powder properties.

Trade Name	Manufacturer	Crystal Structure	d ₅₀ [μm]	BET [m ² /g]	Solids Loading of the Slurry [vol.-%]
HPA 0.5	Ceralox	α-Al ₂ O ₃	0.5	8.9	55
Taimicon TM-DAR	Taimel	α-Al ₂ O ₃	0.2	14.2	45
Disperal S	Condea	γ-AlOOH	0.045	233	10

Lateral shrinkage was determined by comparing the length of a specific structure in micrographs of the template and on the samples in the green and in the sintered state. The densities were measured by the Archimedes method in water.

Received: December 3, 1998
Final version: February 22, 1999

- [1] V. F. Janas, A. Safari, *J. Am. Ceram. Soc.* **1995**, *78*, 2945.
 [2] K. Lubitz, A. Wolff, G. Preu, *Proc. 1993 IEEE Ultrasonics Symp.* **1993**, 515.
 [3] R. Knitter, E. Günther, C. Oedemer, U. Maciejewski, *Microsyst. Technol.* **1996**, *2*, 135.
 [4] W. Bauer, H.-J. Ritzhaupt-Kleissl, J. H. Hausselt, *Microsyst. Technol.* **1998**, *4*, 125.
 [5] H.-J. Ritzhaupt-Kleissl, W. Bauer, E. Günther, J. Laubersheimer, J. Hausselt, *Microsyst. Technol.* **1996**, *2*, 130.
 [6] U. Bast, D. Cramer, A. Wolff, *Ceramics Today—Tomorrow's Ceramics* (Ed: P. Vincenzini) **1991**, *66C*, 2005.
 [7] A. Kumar, H. A. Biebuyck, G. M. Whitesides, *Langmuir* **1994**, *10*, 1498.
 [8] R. J. Jackman, J. L. Wilbur, G. M. Whitesides, *Science* **1995**, *269*, 664.
 [9] H. A. Biebuyck, N. B. Larsen, E. Delamarche, B. Michel, *IBM J. Res. Dev.* **1997**, *41*, 159.
 [10] E. Delamarche, A. Bernard, H. Schmid, B. Michel, H. A. Biebuyck, *Science* **1997**, *276*, 779.
 [11] Y. Xia, G. M. Whitesides, *Angew. Chem. Int. Ed. Engl.* **1998**, *37*, 550.
 [12] Y. Xia, G. M. Whitesides, *Annu. Rev. Mater. Sci.* **1998**, *28*, 153.
 [13] A. Kumar, G. M. Whitesides, *Appl. Phys. Lett.* **1993**, *63*, 2002.

Doped Mesoporous Silica Fibers: A New Laser Material**

By Frank Marlow,* Michael D. McGehee,
Dongyuan Zhao, Bradley F. Chmelka, and
Galen D. Stucky*

Several techniques have been developed for making highly ordered periodic mesoporous materials with pore sizes of 20–300 Å.^[1,2] Already in these early studies several proposals were made to apply such mesoporous systems as optical materials^[3] and highly specific chemical sensors.^[4] Many types of materials can be imagined, e.g., combinations of organic molecules and inorganic species, semiconductor clusters^[5] or lattices,^[6] and also encapsulated polymers^[7] or cluster arrangements. These guest/host materials combine high stability of the inorganic host systems,^[2] new guest-structuring mechanisms produced by confinement in well defined pores and a modular composition. This could lead to new nonlinear optical, optical switching or conducting materials.

These composites can be structured hierarchically,^[8–13] leading to optical materials that have desired optical properties due to the electronic states and molecular arrangements, and that have the desired light-propagation properties due to the macroscopic shape of the material. Self-assembly enables the single-step processing of these complex structures of mesoporous materials. Therefore, one can speculate about the self-assembly of a whole laser, optical switch or other device. This would offer the possibility to grow such devices in huge arrays or on supports with complicated structures or patterns. However, until now there has been no practical proof that the quality of the local mesoscopic structures and the macroscopic homogeneity of fi-

- [*] Dr. F. Marlow,^[+] Dr. D. Zhao, Prof. G. D. Stucky
Department of Chemistry
University of California
Santa Barbara, CA 93106, USA
M. D. McGehee
Department of Materials
University of California
Santa Barbara, CA 93106 (USA)
Prof. B. F. Chmelka
Department of Chemical Engineering
University of California
Santa Barbara, CA 93106 (USA)

[+] Present address: Max-Planck-Institut für Kohlenforschung, D-45470 Mülheim an der Ruhr (Germany).

** The authors would like to thank V. Srdanov, S. Buratto, S. Cordero, J. Y. Park, D. Margoese, P. Yang, and A. Heeger for their support and helpful discussions. This work was supported by the German Science Foundation (DFG, Ma1745/3-1), the National Science Foundation (MRL Program Award No. DMR-96-32716, grants DMR-9257064 and DMR-95-20971) and DARPA (DAAG-55-97-10372).

bers or films of mesoporous materials could be sufficient to realize any desirable optical or electronic function.

In this paper, we demonstrate that the fabrication of a laser based on mesoporous fibers is possible. We show the amplification of a guided mode in the fiber and the resulting directional, gain-narrowed emission. This demonstrates for the first time that mesostructured systems can be applied as advanced optical materials.

There have been a number of encouraging results recently published on new laser materials based on organic thin films,^[14,15] polymers^[16] or glass-like guest/host materials.^[17,18] For polymers, for example, microcavity, micro-ring and distributed feedback lasing have been demonstrated.^[16] However, there are photothermal and photochemical problems that have not yet been solved. The well defined structures of crystalline molecular sieves have, therefore, been used as ordered hosts for new laser materials. Recently, laser properties have been observed for Pyridin 2 dye molecules incorporated in microporous $\text{AlPO}_4\text{-5}$.^[19] In this composite, however, an amplified mode was only detected by scattering effects in selected, occasionally produced whispering gallery resonators. Important advantages of the system presented here are the much larger dimensions of the mesopores, the low temperature synthesis of silica mesostructures using acid synthesis chemistry^[3] and the ease of processability of mesoporous materials to give desired wave-guiding or resonator structures essential for optical devices. The mesopores allow a wide choice of dyes and the tuning of the guest/host system after synthesis by introducing co-adsorbates.

An important step for electronic or optical applications of porous materials is the development of film- and fiber-processing techniques.^[8-11] Researchers have used spontaneous growth mechanisms,^[3] as well as conventional fiber-drawing from solutions, dip coating or spin coating.^[20] For the present investigation, the single-step synthesis of the dye-loaded fibers was based on a procedure previously described in the literature,^[3] and modified to obtain homogeneous fibers. The composition of the initial aqueous synthesis mixture was, e.g., (in mol): $100 \text{ H}_2\text{O} : 0.0246 \text{ CTAB} : 2.92 \text{ HCl} : 0.00017 \text{ Rh6G}$, which was prepared with stirring. $\text{CH}_3(\text{CH}_2)_{15}\text{N}(\text{CH}_3)_3\text{Br}$ (CTAB) was used as the cationic surfactant, in conjunction with the cationic dye rhodamine 6G (Rh6G). 0.05 mol of the silica source reagent $(\text{C}_4\text{H}_9\text{O})_4\text{Si}$ (TBOS) was added to the solution without stirring to form a thin layer on top of the aqueous phase. After 2 days at room temperature, the spontaneous growth of the fibers was observed in the water phase. After 5 days, the fibers were removed from the solution and dried in air. Based on X-ray diffraction, electron microscopy and adsorption measurements, the fibers were determined to have hexagonally ordered mesostructures of cylindrical aggregates with a uniform mean diameter of 22 \AA .^[3] The concentration of Rh6G in the red-colored fibers was about 0.15 wt.-%, as determined by optical absorption measurements on individual fibers.^[21]

The preparation conditions were optimized to maximize the homogeneity of the fibers and, thereby, prevent scattering of waveguided light in the fibers. In Figure 1a one of the fibers is shown. Typically, the fibers display thickness fluctuations of less than 5 % per $100 \mu\text{m}$. In Figure 1b the birefringence of the fibers is analyzed, the fluctuations of which along the length of the fiber are less than 10%. By a similar technique, the absorption of the fibers can be investigated, which yields absorption fluctuations also smaller than 10%. Thus, these fibers have a relatively uniform thickness, absorption and birefringence along the fiber length and they are, therefore, well suited as waveguides.

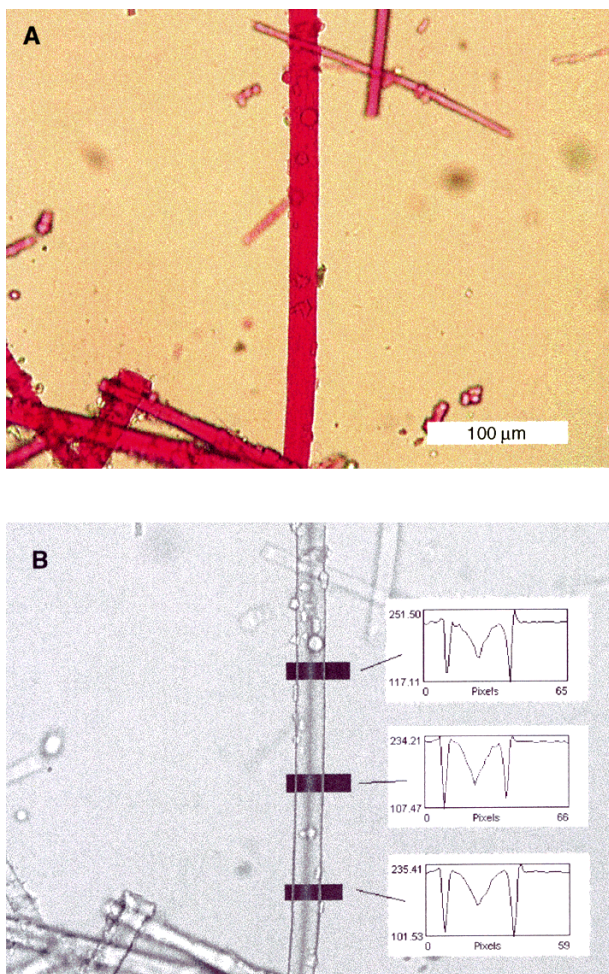


Fig. 1. Optical microscope images of A) a fully transparent fiber in transmission of normal light and B) the same fiber between two parallel polarizers in transmission of red light (700 nm). The fibers have a circular cross section showing no visible inhomogeneities. In B), the fiber forms an angle of 45° with the polarizers. This setup leads to interference effects, revealing that the fibers are birefringent. Here, the interference of ordinary and extraordinary waves in the fiber results in the dark line in the middle of the fiber, which can easily be quantified by the transmission profiles shown in the insets. These transmission profiles can be analyzed to calculate the birefringence [22]. This method provides a spatially resolved overview of the birefringence over the fiber. At the fiber axis, the birefringence was determined to be $n_e - n_o = 0.014$.

In fluorescence investigations the samples were pumped by a frequency-doubled Nd:YAG laser (532 nm , 10 Hz ,

10 ns). The energy of the pulses was controlled using a set of calibrated neutral density filters. An adjustable slit and a cylindrical lens were used to shape the beam into a stripe with a width of 0.3 mm and a length of 1 mm. The slit was also used to select a uniform region of the YAG laser beam. The emission spectra were detected perpendicular to the exciting beam using a grating spectrometer equipped with a thermoelectrically cooled charge coupled device (CCD) detector. The spectra taken are averages of 5, 10 or 50 excitation pulses. The scattered light of the pump laser at 532 nm was suppressed by a notch filter.

In Figure 2A the fluorescence spectrum of a random fiber sample is shown for different pumping powers. At low excitation power, one observes a broad (65 nm) spectrum typical for rhodamine. The spectral band shape results from the pure fluorescence and reabsorption losses in the dyedoped fiber. As the pump power is increased, one first observes small shifts in the fluorescence maximum and an increased short-wavelength tail (not shown). These effects can be assigned to altered reabsorption due to depopulation of the ground state. Above a threshold of about 2400 kW/cm², a gain-narrowed peak rises out of the broad spectrum.^[23] This phenomenon is well-known and can be attributed to amplified spontaneous emission, a process by which spontaneously emitted light is amplified by stimulated emission.^[24] The typical full width at half maximum (FWHM) of the gain-narrowed peak is between 7 and 10 nm. The intensity behavior of this peak is shown in Figure 2B. It is worth noting that this peak arises at pumping powers at least one order of magnitude higher than those pumping powers at which the small spectral shifts attributed to ground state depopulation effects have been observed.

In order to reduce the threshold for gain narrowing, it is important to pump a fiber homogeneously and to detect the emission from the end of the fiber nearly parallel to its longitudinal axis. In this arrangement the emitted light travels a long distance in the gain medium and can therefore be significantly amplified, even when the gain is small. Figure 3 shows the fluorescence of a single fiber observed from one of its end faces. The fiber is excited perpendicular to the axis and absorbs about 35 % of the pump intensity. Only at small excitation densities does one find a spectrum comparable to the radial fluorescence, but slightly modified by the stronger reabsorption effects. Above excitation densities of 15 kW/cm², the band narrows significantly and increases in intensity much faster than the excitation power (Fig. 3B). The minimum width for the band was 7 nm, which is comparable to the amplified spontaneous emission of other materials.^[24] Both the nonlinear intensity behavior and the narrowing of the band are typical properties of a high-gain laser material when pumped without a resonator.

A further property of the narrow-band emission is the beam-like distribution of the output, which is shown in Figure 4. The output beam can be characterized by its wavelength and by the deviation of its orientation relative to the

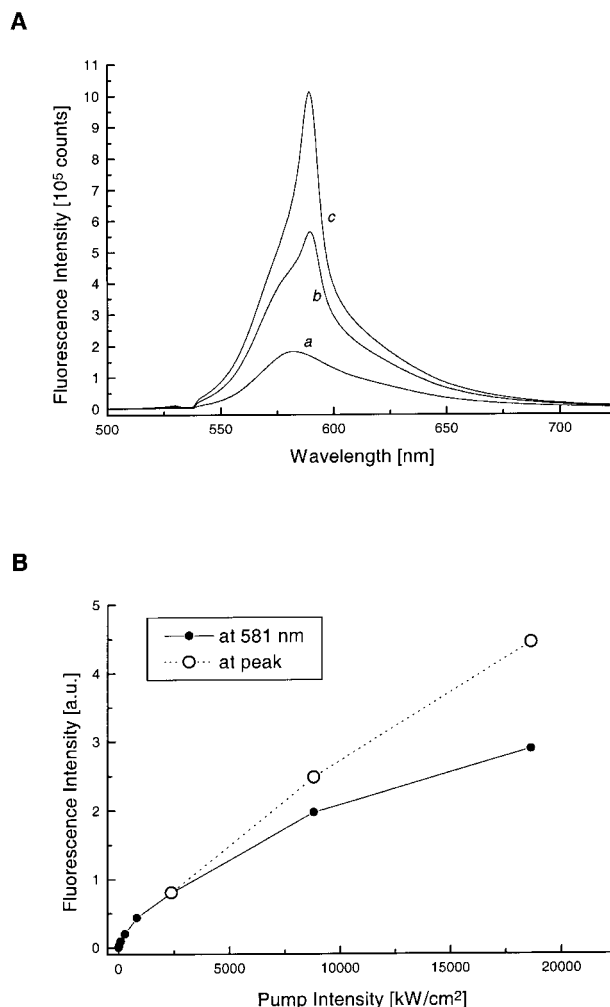


Fig. 2. A) Fluorescence spectra of a random fiber sample at different pump intensities (a: 2400 kW/cm², b: 8000 kW/cm², c: 18000 kW/cm²) [23]. Below 2400 kW/cm² there are only slight changes in the spectrum. The fibers were placed between two glass slides separated by 0.1 mm, so that the fiber axes lie in the plane of the glass slides for these random fiber samples. The plane of the sample forms an angle of about 40° with the incident light and the fluorescence is detected perpendicular to the incident light. This measurement setup allows the detection of fluorescence radiation escaping from the fibers in nearly radial directions only (i.e., angles between 30° and 150° with respect to the fiber axes). Since the fibers are thin (thickness between 5 and 25 μm), the path length for amplification of fluorescence radiation is small, resulting in a high threshold for this radial amplified spontaneous emission visible in spectra b and c. B) Intensity dependence of the fluorescence of a random fiber sample. Lines are shown to guide the eye. At low excitation densities, the fluorescence maximum is at about 581 nm. The gain-narrowed peak arises at 589 nm.

fiber axis described by the angle α . Figure 4 shows a very narrow ($\pm 4^\circ$) angular intensity distribution of the narrow-band emission. Based on these observations, one can call the emission phenomenon mirrorless lasing. We do not think that resonant feedback plays a significant role in the described phenomena. The gain-narrowed emission has been observed even when the quality of the fiber faces was poor and when the fibers were embedded in grease. All of these effects are understandable with regard to amplified spontaneous emission only. We remark that the intensity of the mirrorless lasing output is surprisingly large above the

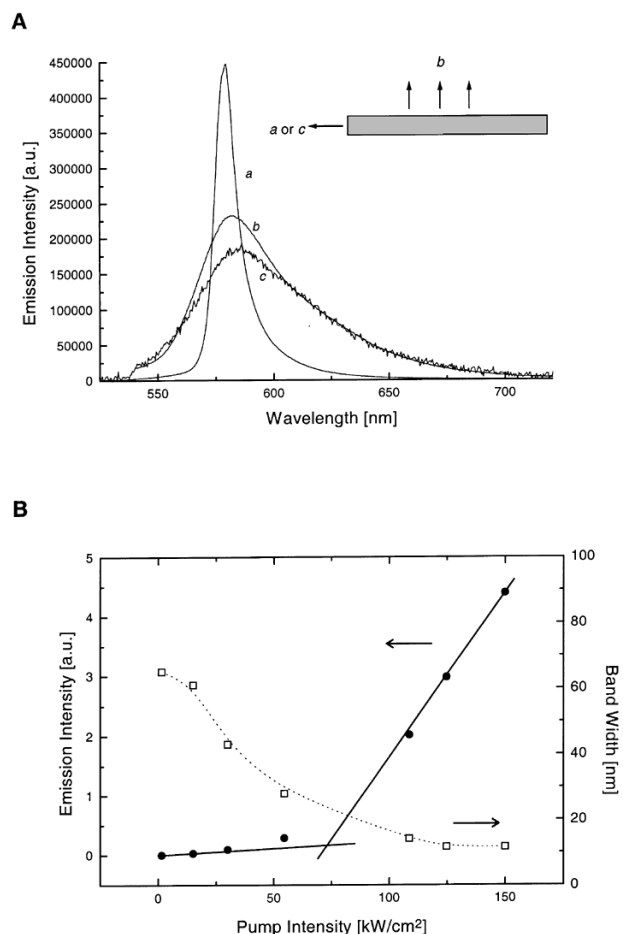


Fig. 3. A) Fluorescence spectra of a single fiber (diameter 10 μm , length 300 μm) measured parallel to the fiber axis. The pump laser beam was perpendicular to the fiber axis. Curve a is the gain-narrowed spectrum at 150 kW/cm^2 . Curve b represents the radial emission for comparison. Curve c is the axial emission at lower pump intensities (15 kW/cm^2). B) The intensity dependence of the axial single fiber emission [23]. The full circles (●) are the emission intensity at the peak and the open squares (□) are the band width (FWHM). The solid straight lines indicate the low intensity and the high intensity behaviors. The dotted curve is shown to guide the eye.

threshold. The output beam is easily visible, as shown in Figure 5.

The very narrow angular distribution of the output radiation shown in Figure 4 can be explained by the amplification of the lowest waveguide mode only, which has a theoretical output divergence of about 4°. This is much less than the acceptance angle of the mesoporous fiber waveguide which is at least 20° when one assumes that the fiber acts as multimode step-index waveguide. Very likely, the damping of the different modes in the fiber depends on the field strength at the fiber boundary, because it is slightly scattering. This results in a lower damping of the low-order modes present in the fiber that are connected with the more collimated output beams.

Rh6G-containing composites are a relatively simple type of laser material. However, these composites demonstrate that the chosen host system is potentially suited for other

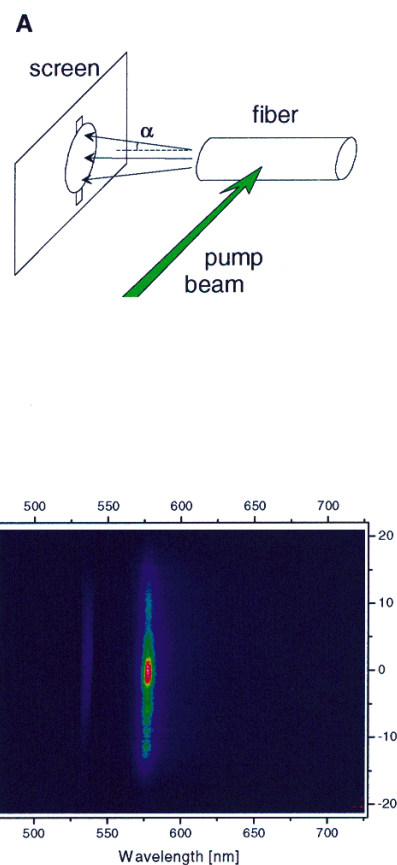


Fig. 4. A) Schematic diagram of the far field measurement of the gain-narrowed emission. The fiber output is scattered by a frosted glass screen which is projected on the entrance slit of an imaging monochromator that has a CCD camera at the exit. Each ordinate value of the CCD-image shown in B) represents a different radial position of the far-field spot. These positions have been recalculated as deviation angles α with respect to the fiber axis. The abscissa values correspond to the wavelength λ as in a typical spectrum. The pseudo color CCD image shows a large intensity only in a narrow angle sector. This means that the spectrally narrow fiber emission is nearly collimated parallel to the fiber axis. A fiber of 8 μm diameter and 150 μm length has been used here.

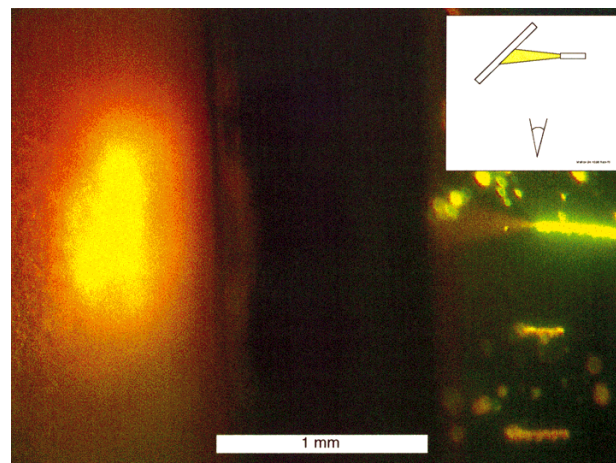


Fig. 5. Photograph of the output beam and the emitting fiber. As indicated in the inset a screen has been placed about 2 mm away from the fiber end to show the output beam. The picture was taken during a single excitation pulse. The beam is clearly visible above threshold.

types of lasing guests, such as rare earth complexes or conjugated polymers. The requirements concerning homogeneity and material shape can be fulfilled. These other types of light-emitting species are now being investigated for incorporation into mesoporous hosts in order to construct laser materials. This new class of materials offers many possible variations according to the selection of luminescent species or coadsorbates to extend the wavelength range of emission and excitation. The self-assembled host, especially, allows appreciable control of mesoscale dimensions, symmetry and orientational ordering of guest-host structures. Energy transfer might be exploited for sensitizing a dye or for exciting narrow-line emitters, such as rare-earth complexes. Saturable absorbers could also be incorporated in the composite to make ultrafast lasers. These composites provide versatile opportunities for the construction of efficient and tunable new laser materials. Further options in using mesoporous host materials for lasing guests are to use them as highly sensitive sensors^[25] where the lasing wavelength is varied, for example, by gas adsorption.

Received: January 18, 1999

- [1] C. T. Kresge, M. E. Leonowicz, W. J. Roth, J. C. Vartuli, J. S. Beck, *Nature* **1992**, 359, 710.
- [2] See e.g.: D. Zhao et al., *Science* **1998**, 279, 548.
- [3] Q. Huo, D. Zhao, J. Feng, K. Weston, S. K. Buratto, G. D. Stucky, S. Schacht, F. Schüth, *Adv. Mater.* **1997**, 9, 974.
- [4] C. Gojon, B. Dureault, N. Hovnanian, C. Guizard, *Sens. Actuators B* **1997**, 38, 154.
- [5] R. Leon, D. Margolese, G. Stucky, P. M. Petroff, *Phys. Rev. B* **1995**, 52, R2285.
- [6] D. M. Antonelli, J. Y. Ying, *Angew. Chem., Int. Ed. Engl.* **1995**, 34, 2015. P. V. Braun, P. Osenar, S. I. Stupp, *Nature* **1996**, 380, 325. P. Yang, D. Zhao, D. Margolese, B. F. Chmelka, G. D. Stucky, *Nature*, in press.
- [7] C. G. Wu, T. Bein, *Science* **1994**, 266, 1013.
- [8] P. J. Bruinsma, A. Y. Kim, J. Liu, S. Baskaran, *Chem. Mater.* **1997**, 9, 2507.
- [9] P. Yang, D. Zhao, B. F. Chmelka, G. D. Stucky, *Chem. Mater.* **1998**, 10, 2033.
- [10] H. Tamai, M. Ikeuchi, S. Kojima, H. Yasuda, *Adv. Mater.* **1997**, 9, 55.
- [11] H. Yang, A. Kuperman, N. Coombs, S. Mamiche-Afara, G. A. Ozin, *Nature* **1996**, 379, 703. H. Yang, N. Coombs, I. Sokolov, G. A. Ozin, *Nature* **1996**, 381, 589. I. A. Aksay et al., *Science* **1996**, 273, 892. M. Ogasawa, *J. Am. Chem. Soc.* **1994**, 116, 7941. S. H. Tolbert, T. E. Schäffer, J. Feng, P. K. Hansma, G. D. Stucky, *Chem. Mater.* **1997**, 9, 1962.
- [12] M. Trau et al., *Nature* **1997**, 390, 674. P. Yang et al., *Science* **1999**, 282, 2244.
- [13] S. Mann, G. Ozin, *Nature* **1996**, 382, 313.
- [14] V. G. Kozlov, V. Bulović, P. E. Burrows, R. S. Forrest, *Nature* **1997**, 389, 362.
- [15] M. Berggren, A. Dodabalapur, R. E. Slusher, Z. Bao, *Nature* **1997**, 389, 466.
- [16] M. D. McGehee et al., *Appl. Phys. Lett.* **1998**, 72, 1536. F. Hide et al., *Science* **1996**, 273, 1833. N. Tessler, G. J. Denton, R. H. Friend, *Nature* **1996**, 382, 695.
- [17] D. Shamrakov, P. Reinfeld, *Chem. Phys. Lett.* **1993**, 213, 47.
- [18] D. Lo, J. E. Parris, J. L. Lawless, *Appl. Phys. B* **1992**, 55, 365.
- [19] G. Ihlein, F. Schüth, O. Krauss, U. Vietze, F. Laeri, *Adv. Mater.* **1998**, 10, 1117.
- [20] D. Zhao, P. Yang, N. Melosh, J. Feng, B. F. Chmelka, G. D. Stucky, *Adv. Mater.* **1998**, 10, 1380.
- [21] F. Marlow et al., *Micropor. Mater.* **1996**, 6, 43.
- [22] This method has been used for microcrystals, for example: K. Hoffmann, F. Marlow, J. Caro, *Adv. Mater.* **1997**, 9, 567.
- [23] Here, we use the mean intensity of the 10 ns pulses to describe the pump radiation. So, 100 kW/cm² corresponds to 1 mJ/(cm²·pulse).
- [24] See e.g.: M. D. McGehee et al., *Phys. Rev. B* **1998**, 58, 7035.
- [25] T. A. Dickinson, J. White, J. S. Kauer, D. R. Walt, *Nature* **1996**, 382, 697.

Radial Patterns in Mesoporous Silica**

By Igor Sokolov, Hong Yang, Geoffrey A. Ozin,* and Charles T. Kresge

It has been found that in a surfactant-templated quiescent aqueous acidic synthesis of hexagonal mesoporous silica, three basic shapes can be formed with increasing pH, respectively fibers, discoids and spheres.^[1–6] Intriguing radial patterns that have been observed on the surface of some of these shapes have defied explanation. It is considered that morphogenesis of mesoporous silica shapes is initiated by topological defects in a hexagonal silicate liquid crystal seed.^[1–6] For instance, under conditions that favor a 2π -line disclination and a discoid shape for the nucleating silicate mesophase, the director field whirls concentrically and coaxially around the defect line. The surface mesostructure and zeta potential of this embryonic silicate discoid serves to direct the silicification and growth of mesoporous silica to a discoid shape.

Herein we show that the classical theory of elasticity for liquid crystals^[7] can be used to minimize the bulk and surface free energy of a hexagonal silicate mesophase containing a 2π -line disclination defect. These calculations reveal the emergence of radial patterns that bear a striking resemblance to those observed on the surface of mesoporous silica discoids. It is noted that silicification and contraction of the silicate mesophase can impose radial and longitudinal compressive stresses on the discoid. The compressive strain may be dissipated by corrugation of the disclination making it more visible. Depending on the relative rates of polymerization of the silicate core and corona, the strain may also be released by deforming the flat discoid to create protruding or sunken discoid shapes.

An insight into the mode of formation of hexagonal mesoporous silica fiber, discoid and sphere shapes has been obtained from scanning and transmission electron (SEM, TEM), atomic force (AFM), and polarization optical microscopy (POM). These techniques define the relation between the pattern of channel director fields, optical birefringence and morphology, and hence provide clues about the growth process of a particular form.^[1–5]

Morphokinetic, dynamic light scattering, TEM and AFM studies of the formation of different mesoporous silica

[*] Prof. G. A. Ozin, Dr. I. Sokolov, Dr. H. Yang
Materials Chemistry Research Group
Chemistry Department, University of Toronto
80 St. George Street
Toronto, Ontario, M5S 3H6 (Canada)
Dr. C. T. Kresge
Mobil Technology Company
Paulsboro, New Jersey 08066-0480 (USA)

[**] GAO is indebted to the Canada Council for the award of an Issac Walton Foundation Research Fellowship 1995–97 that was held during this research. GAO is also deeply grateful to the Mobil Technology Company for financial support of this research. Technical discussions with Prof. Raymond Kapral proved to be most enlightening.